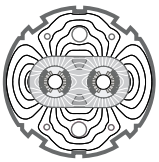

LHC Project Note 238

2000-10-12

Ana.Arauzo.Garcia@cern.ch

Configuration of the Beam Loss Monitors for the LHC arcs

Author(s) / Div-Group:Ana Arauzo Garcia, Bernd Dehning / SL-BI

Keywords: Beam loss, beam loss monitors, quench protection

Abstract

A revised configuration for a beam loss detection system is given for the arcs of the LHC. The last modifications of the LHC arc layout have been taken into account, LHC optics version 6.2. A set of 6 Loss Detectors will be placed outside the cryostat around each short straight section. Quench alarm thresholds are estimated for each detector in all possible LHC arc layout configurations. Threshold values are proposed for top and injection energy beam loss.

1. Introduction

In previous studies [1,2], a beam loss detection system has been proposed for the LHC arcs. Protons from beam losses scraping the beam pipe in the most likely aperture limitations were considered. In these papers [1,2], the Monte Carlo shower code GEANT 3.21 [3] has been used to simulate the impact of high energy protons (point losses) on the aperture of superconducting magnets. These calculations allow determining the sensitivity of Beam Loss Monitors (BLM) for the LHC, as well as, the suitable locations and the number of monitors.

Protons with large betatronic amplitudes will most likely hit the beam screen at a maximum value of the horizontal or vertical beam envelope. The incident proton interacts with a nucleus of the beam screen or other material like the beam pipe or coil. As the shower develops through the material surrounding the beam pipe, the produced particles lose energy in inelastic interactions with atoms along their track. The distribution of secondary particles outside the cryostat is maximum at a certain distance of the incidence point. The intensity, longitudinal shape and position of the shower depend on the amount and type of material the particles traverse.

The geometry used in the simulations contains the Short Straight Section (SSS) with a twin-aperture quadrupole, two octupoles, and two combined sextupole-dipole corrector (MSCB) magnets, as well as surrounding dipoles plus correctors. In this paper, the geometry is updated using the last released layout for the LHC arcs, following LHC optics version 6.2[1] [4,5,6,7].

The arc-cell geometric configuration is simplified for the calculations. The main changes of the geometry from last version concern the corrector magnets [7]. All previous

[1] The general LHC arc-cell layout does not change from version 6.1.

calculations have been revised and recalculated. A more complete study has been made by varying the incident proton energy. Most of the general results obtained before are still valid. Nevertheless, in view of the new results, the proposal for the Beam Loss Monitor system has been slightly changed. The number of detectors needed for quench control remains the same, only some of the positions and thresholds have been modified.

2. Geometry and Procedure

2.1. LHC half-cell geometry description

The geometry used in the simulations corresponds to a Short Straight Section (SSS) of the LHC arcs. The layout and the different elements configuration and description is based on optics version 6.2.

The SSS of the half-cell consists of a main twin aperture quadrupole magnet (MQ), plus correctors. The coordinate system origin is in the centre of the MQ, and only the flanked Main Dipoles (MD), plus the corresponding corrector magnets, are defined. The geometry has been simplified to avoid an excessive number of interfaces, which would enormously complicate the program handling and increase the computing time.

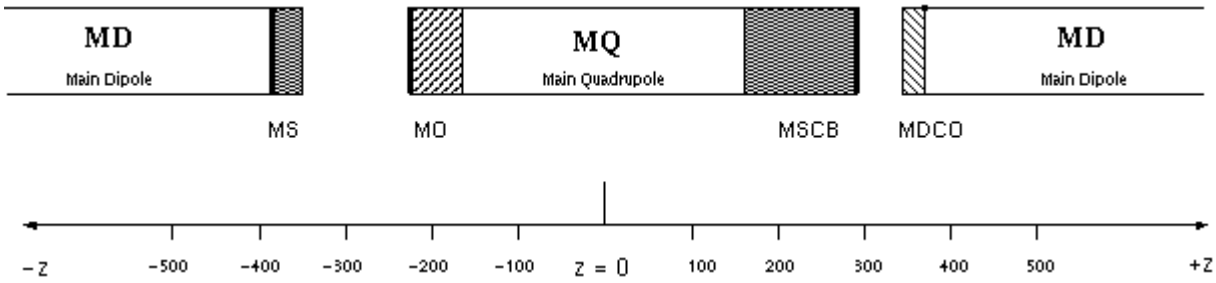

Fig. 1. Detail of the SSS half-cell geometry used for the simulations. The longitudinal configuration includes the quadrupole (MQ), the dipoles (MD) and corrector magnets (z values are in centimetres).

In Fig. 1, the scheme of the general simulated configuration for the LHC half-cell is plotted. The longitudinal extension covers both adjacent Main Dipoles.

In the LHC standard arc, there are several types of Short Strait Section (SSS) from the magnetic element Q12L to Q12R. A total of 62 different SSS types are identified [5]. They differ in the magnet combination, front cover type, MQ diode, vacuum barrier, phase separator and technical service module. For our purposes, several of the SSS can be simplified. We consider only the variety of different magnet combination. The other elements do not play an important role in the material configuration and they are highly simplified in the simulated geometry.

The magnet configuration for the SSS includes the MQ (Focalising or Defocalising, F or D), the Sextupole-Dipole corrector (MSCB) type A, B, C or D and an additional corrector magnet. The latter can be an Octupole (MO), a Skew Quadrupole (MQS) or a Tuning Quadrupole (MQT).

In the GEANT cascade simulations, the main factor is the amount of dense matter. Therefore, small differences in configuration will not be taken into account if the material amount and composition is similar. Following this assumption, the MSCB magnets are all equivalent and only the differences in the corrector magnet, MO, MQS or MQT have been studied.

In the last version of the SSS the cold mass in the cryostat has been increased as much as possible in order to reduce the amount of liquid Helium needed to fill the vessel. The MQ correctors have been equipped with a voluminous iron support and some small spaces left will be almost entirely occupied by radiation-hard polyethylene filling pieces. As a consequence, the differences between the MO, MQS and MQT correctors are masked by the support. We have considered only the case of the MO which, is the most frequently used in the arcs.

The SSS types are in this way reduced to only two types, SSS with the MQ magnet focusing or defocusing.

The LHC MD magnets are equipped with Decapole and Octupole corrector magnets (MCDO) and Sextupole corrector magnets (MCS). In version 6.2 (already 6.1) the MDCO is only present at every second MD [6]. As a consequence we have to consider the arc layout with and without the presence of the MDCO corrector.

2.2. Quench levels for point losses

The number of lost protons that lead a magnet to quench has been computed for different loss duration [8]. For a medium range loss time (lasting 10 milliseconds) the number of lost top energy protons which induces a quench in the magnet is of the order of 10^7 (for local or for distributed losses). At injection energy a quench is produced with 10^9 lost protons. A loss detection system must be able to detect much smaller losses than that leading a magnet to quench. Last values are given with a safety margin of ±50 % [10].

The beam loss monitors layout is designed by analysing where the losses can occur. During the operation with colliding beams, the losses are concentrated in the cleaning sections. Beyond the cleaning sections, there are still some protons whose betatronic amplitude is larger than the aperture of the ring, forming the tertiary halo. These protons will be scraped by the bottlenecks of the beam screen. Along a cell, aperture limitations are located near the quadrupoles where the betatronic functions have a maximum value. In addition, the misalignment error between the SSS and the MD beam screen (SSS-MD and MD-SSS interconnections) has to be taken into account. The alignment accuracy allows relative beam screen displacement by a maximum of 3-mm peak to peak. It has been shown [9] that most losses will occur in the first half of the quadrupole and misalignments can produce losses in the upstream dipole and in the interconnection with the downstream dipole.

For most of the particle shower estimates, a localised proton impact was generated. To evaluate the effect of distributed losses a set of point losses have been calculated and then integrated over the distribution loss extension.

2.3. Point loss initial conditions and loss detection outside the cryostat

The conditions and assumptions made for simulating beam losses are as in previous calculations [1,2]. We assume losses are produced in the arc half-cell where the ß function is at his maxima, in the centre of the focusing MQ. The loss will occur at the beam screen in the horizontal plane for a horizontally focusing MQ (QF), and in the vertical plane for a vertically focusing MQ (QD). Loss may happen at both beam screen sides. Thus, a loss is considered in the horizontal case, for the innermost and the outermost point of the beam screen. Respectively in the vertical case, the loss may happen on the uppermost (top) and the downermost (bottom) point.

Fig. 2 shows the cross-section of a QD magnet as defined in the simulations. A point loss has been produced in the left beam and the first tracking steps of the first originated secondaries have been also plotted. The proton is lost in the outermost point of the beam screen.

Losses are considered at the longitudinal positions z = -325 cm, 0 cm, +325 cm. These positions correspond to the end of the upstream dipole beam screen, the centre of the quadrupole, and the beginning of the beam screen for the downstream dipole. The *z* co-ordinate of the hitting point is called vertex or z_v.

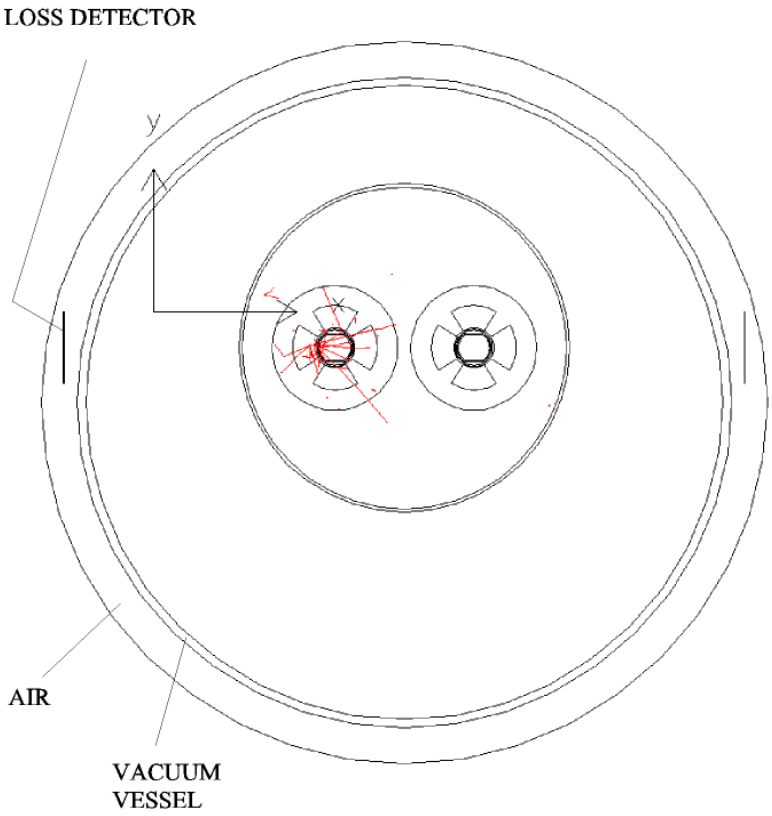

Fig.2. Cross-section of the SSS at the MQ location. This drawing is an output of the GEANT 3.21 drawing package showing the main components of the simulated geometry. In red, the first steps of the cascade due to a point loss on the beam screen are shown.

The calculation procedure consists of, relating the number of lost protons in a local point of the beam screen with the number of produced particles outside the cryostat in any longitudinal position. The detection system is foreseen to be made up of PIN diodes positioned outside the cryostat. PIN diodes are sensitive to the passage of Minimum Ionising Particles (MIPs).

To obtain the number of MIPs which leave the vacuum vessel, two theoretical loss detectors have been placed outside the cryostat, on both sides. These are in air to reproduce the real set-up (see Fig. 2). Both loss detectors consist of an aluminium foil with dimensions: thickness = 0.05 cm, height = 10 cm and length = 3600 cm. They act as targets counting the particles going through them. For a loss in either of the beams, the generated cascade is observed in both detectors. We obtain, in addition to the signal in the nearest detector also a signal in the detector situated at the opposite side of the vessel, the so called 'cross-talk' signal.

2.4. LHC half-cell configurations

Given the geometrical setup for the half-cell, described in section 2.1, we have to consider the different possibilities present in the future LHC ring. After every LHC interaction point, beams interchange the vacuum pipe. Taking the previous analysis into account, from

the SSS types and MD types, we have 8 different combinations. Four of them depend on the MQ and MD polarity and the other four are simply without the MCDO magnet (see Fig.1 and Fig. 3). In case A and B, the beam on the right beam pipe is going in the +z direction, and the beam on the left beam pipe in the –z direction (see Fig. 3, right). The difference between the configuration A and B is the focalisation of the MQ magnet. For the C and D configurations, the sense of the beams is inverted and therefore the magnetic field in the MD.

The values for the bending field in the MD and the focalizing field in the MQ have been calculated with the program ROXIE [12]. Magnetic field has been mapped from the beam pipe centre up to a maximum x and y value of 60 mm. The magnetic field in the correctors is not considered.

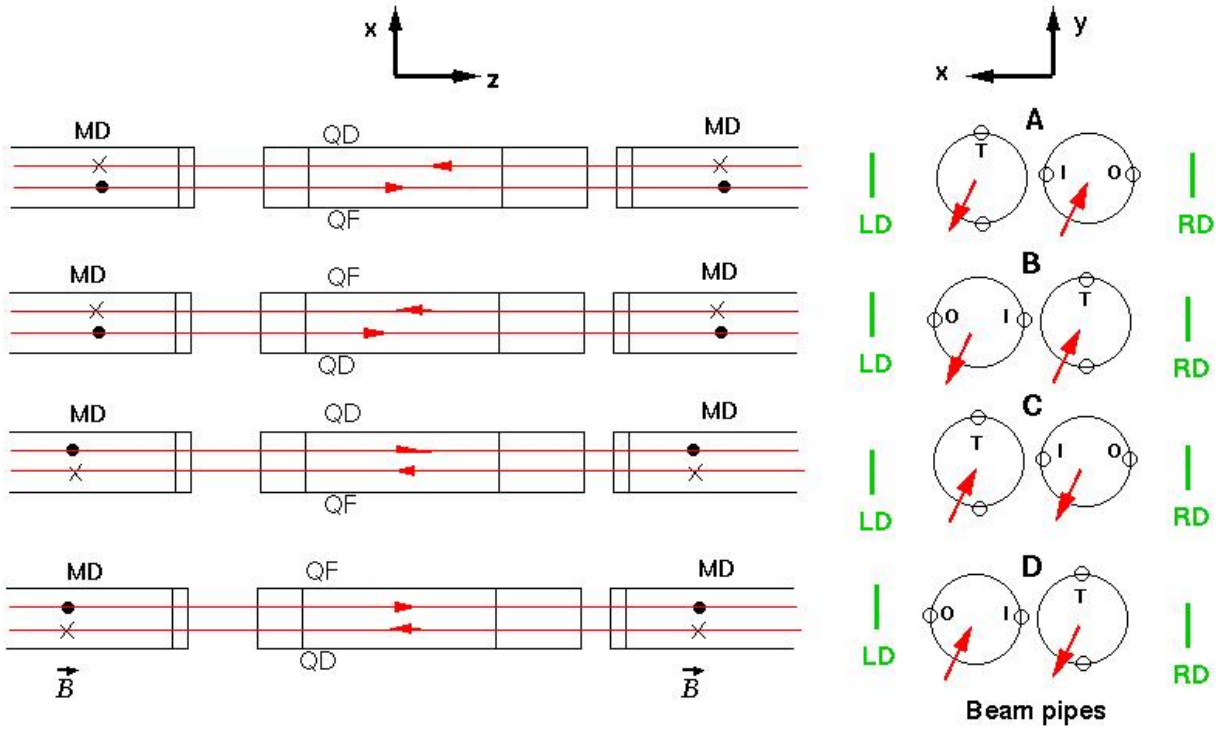

Fig. 3. Schematic representation of the different configurations for the half-cell. View from the top, the arrows indicate the direction of the beams. In the MD magnets, the standard signs indicate the magnetic field. The quadrupole magnets (MQ) are focusing (QF) or defocusing (QD) in the horizontal plane. On the right, the different locations of point losses are shown for each beam pipe; ***T*** *means Top,* ***I*** *means Innermost and* ***O*** *means Outermost.*

For all of these geometrical configurations, the point losses in the transversal positions (Fig. 3 right) are considered. In addition simulations were executed for the three likely longitudinal loss locations (z_v = -325, 0 and +325 cm). The loss in the bottom of the beam screen is not analysed because it is equivalent by symmetry to the top case loss.

The loss detectors are named as shown in Fig. 3, right. RD for the detector at the right and LD for the detector at the left. In the standard reference system for circular accelerators, LD is located in the external part of the ring and RD in the internal part of the ring.

3. Results

The obtained shower distributions along the beam direction show similar general features as with previous analysed layout [1,2]. The distribution starts approximately at the interaction point. It increases sharply to a maximum value about 1m far downstream from the point loss location. It decreases softly in the direction of the beam, but it is drastically modulated by the amount of lateral material.

The characteristics of the cascade distributions were already explained in detail in previous papers, therefore, this paper is focused on the new analysis and results.

The main differences of the new calculations are:

- The massive support introduced for the MQ correctors: MO and MSCB and the plastic filling pieces. The differences between intermagnet gaps to the left and right of the SSS are now larger.
- The MQ quench diode and BPMs definitions have been updated.
- A new configuration without a MCDO corrector in the MD was added.

Moreover, the program has been improved to allow the control of every designed element and therefore reducing the occurrence of design errors.

3.1. Variations with Configuration type

The main differences between results obtained in A, B, C and D configuration are related to the asymmetry of the intermagnet gaps in the SSS (see Figs. 1, 3). When the shower is developed into the gap, the MIP distribution intensity is much higher in the long gap than in the short gap. Moreover, the main signal appears when the shower is developed in the large intermagnet gap. This asymmetry is stronger in the new configuration than in previous results due to the MQ massif correctors. In previous papers, the factor between the signal obtained for a shower in the long gap in respect to the short gap was about 1.5. This factor is doubled in the new version. In general, the MIP distribution intensity is lower for the new version, up to a 50 % less in some cases. The cross-talk signal however has slightly increased and shifted.

Even if results differ from one configuration to the other due to the different type of loss (O, I, T, see Fig.3 right) and the magnetic fields in the MQ and MD, the main features are observed for all the configurations. A and B configurations have very similar results as well as C and D configuration. To compare A&B with C&D they have to be compared with beams travelling in the same direction. The intensity of the obtained MIPs distributions differs however from one configuration to another.

Seen that the behaviour for different configurations is similar for similar conditions, we can reliably extrapolate results for one configuration to the others. Some studies like, the MCDO presence influence, the evaluation of a distributed loss, the cascade mean time of flight and the lost proton energy dependence, have been performed for only one type of configuration.

The study of the arc-cells without the MDCO has been done for the case of an A type configuration. Only point losses at z_v = 325 cm for the beam going in the +z direction are affected by this element. Fig. 4 shows the results obtained for the outermost (left figure) and the innermost (right figure) point loss at z_v = 325 cm, with and without the MDCO corrector. The differences between the distributions are not important taking into account we can not distinguish in a detector from an outermost or an innermost loss on the beam pipe. It can be concluded that the presence of this element is not of major importance in the analysis of beam

loss detection system for different configurations. The number of possible configurations is then reduced to four.

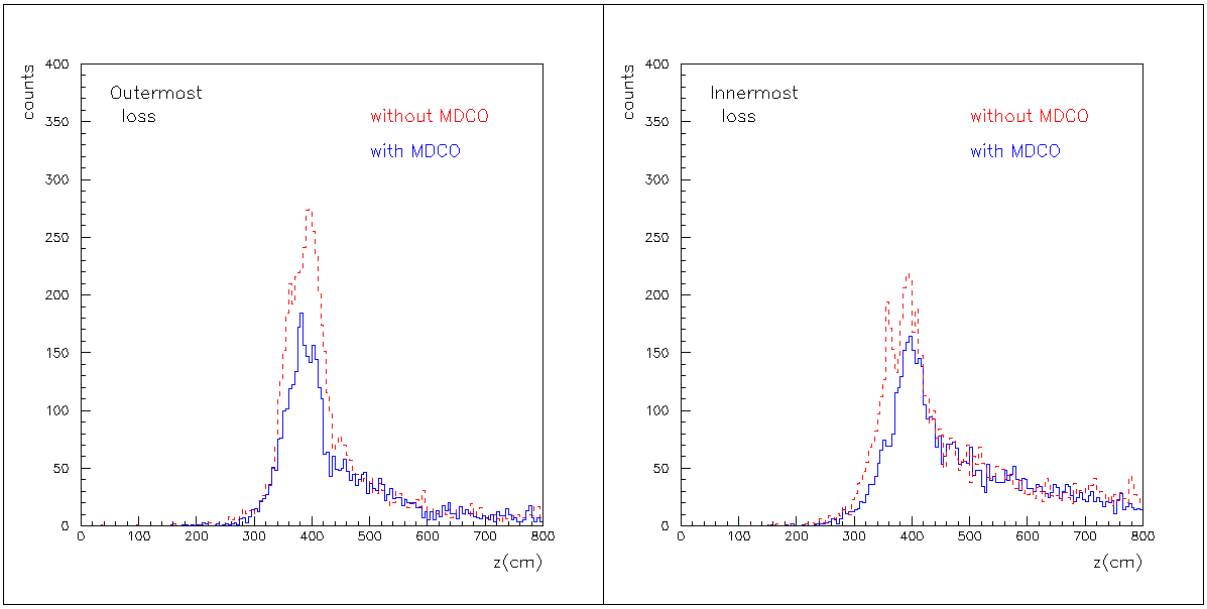

Fig. 4. MIPs distribution obtained for A configuration with and without the MDCO corrector. Point loss at z_v = 325 cm. On the left it is drawn the results for the outermost loss and on the right for the innermost loss.

The studies performed for a distributed loss have similar results than in the previous simulations. A point loss is a good approximation of a distributed loss for most of the cases, being the differences less than 30%. There are only some particular cases in which a distributed loss gives a MIP distribution which is much higher than for a point loss. These cases occur when the loss takes place in the innermost or uppermost part of the beam screen and a part of the distributed loss is within the MD (magnetic field influence [1]). Distributed loss gives a shower with a maximum value a factor 2 or 3 higher than a point loss. The high discrepancy is explained due the strong magnetic field of the MD magnet. Charged particles are bent by the magnetic field and in consequence the number of interactions and the resultant MIP number increases. As a consequence, the MIP distribution changes drastically for a proton lost in the SSS-MD interconnection and for a proton lost in the MD beam screen. In a real situation we expect to have a softer transition for the magnetic field and for the beam losses, therefore, we average the values for the BLM thresholds in this particular case.

In general, the proposal for the placement of the beam loss detectors system takes into account the results from distributed losses. The position for the BLMs has been studied to treat as much as possible the differences between point loss and distributed loss.

After the first interaction, the generated particles travel through the different materials interacting in their turn and creating new secondaries. The arrival time at the detector and the impact time are recorded in order to obtain the shower time of flight, TOF. It is found that the particles reach the loss detector in less than 5 ns. Higher times correspond to the tail of the MIP distribution or to the secondary peaks.

3.2. Variations with proton energy

Simulations have been done in most of the cases for 7 TeV energy protons, for which a large loss and the immediate energy dose deposition along the superconducting magnets have the strongest effects. For the C configuration, simulations were carried out with a proton energy of 450 GeV. We have found that the top to bottom energy signal ratio is different for one point loss to another, ranging from 10 to 25. In order to check the signal intensity evolution with energy, MIP distributions for energies from 0.45 – 7 TeV have been studied.

Fig. 5a shows the obtained MIP distribution for a point loss at different energies. The longitudinal distribution shape does not present noticeable changes for different proton energies.

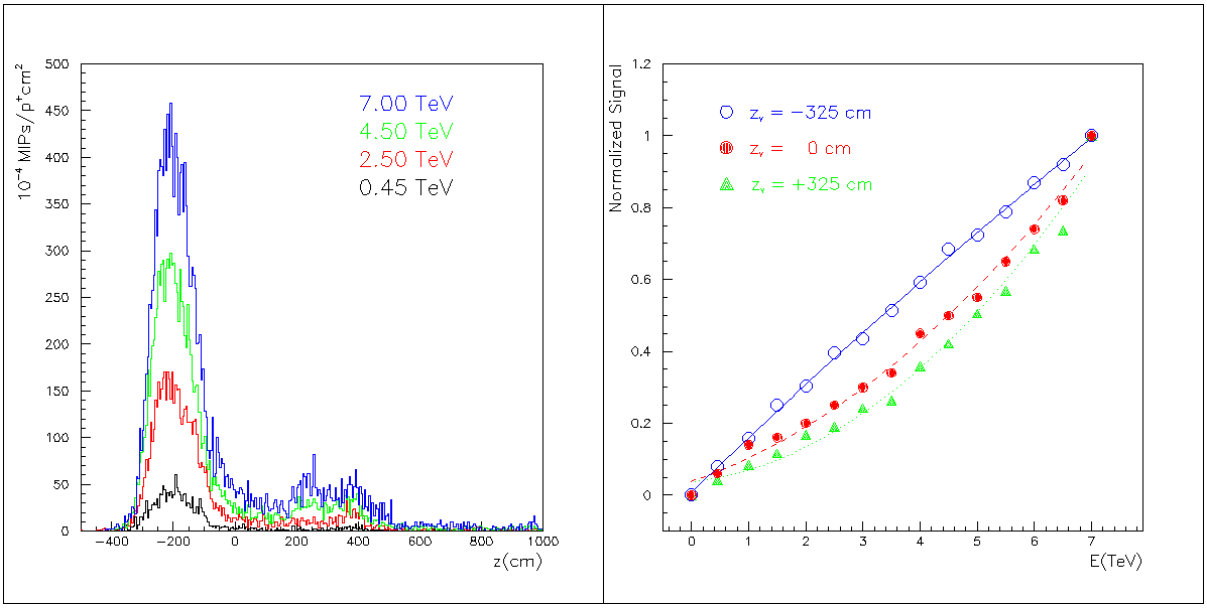

Fig. 5a, 5b. Energy dependence of MIPs distribution. A) Right: MIP distributions for a point loss at z_v = -325 cm obtained for 4 different p^+ energies. B) Left: Energy evolution for three different MIP distributions. The normalised signal corresponds to a selected longitudinal position for each of the distributions, -250 cm for a point loss at z_v = -325 cm, 200 cm for z_v = 0 cm and +450 for z_v = +325 cm.

Fig. 5b shows the energy evolution of the relative MIP distribution signal for three different cases. The dependence goes from linear to a slight quadratic dependence. The data represented correspond to a longitudinal position of the MIP distribution, z = -250 cm for a point loss at z_v = -325 cm, z = 200 cm for z_v = 0 cm, and z = 450 cm for z_v = 325 cm. This position is chosen to be the most suitable for a loss monitor as it is shown later in Tables 1, 2.

In general, for losses in the MQ (z_v = 0 cm) the signal ratio I(7 TeV)/I(450 GeV) is about 15. The ratio is lower (down to 10) for losses developed in the intermagnet gaps and higher (up to 25) for cascades going into the MD.

4. Configuration of Beam Loss Monitors

The most likely candidate for the detection system is PIN diodes. PIN diodes are sensitive to the passage of Minimum ionising particles. For the LHC, 25 ns bunch spacing is a

long time compared to the TOF mean time, 5 ns. With high-rate (40 MHz) PIN diodes it is possible to measure the losses produced by every bunch.

As it was previously concluded [1,2], and in view the new results agree with the old ones, a set of only six BLMs around every quadrupole in the arcs is needed, three BLMs per beam. In reference to the four types of configurations and the used reference system (see Fig. 3), the BLMs are named RD1, RD2 and RD3 for the RDs and LD1, LD2 and LD3 for the LDs. The numbers count in increasing longitudinal position.

A new proposal is made for the positions and thresholds of the BLMs. New results differ not only in the threshold value calculated for the BLM set, but also, in the proposed locations for the detectors. The main reason to change the positions has been to minimise cross-talk signal to allow an almost unambiguous detection of the lost beam.

4.1. BLM Locations

The positions for the beam loss detectors have been chosen taking into account several factors. First, to reduce the differences between an innermost and an outermost loss as they can not be distinguished at the detector. Then, cross talk must be minimised to avoid an ambiguous identification of the beam which suffers from the loss. In addition, the signal due to a distributed loss must agree as much as possible with that of a point loss. All these factors are taken into account to produce Table 1. For the chosen position for the BLMs, the measured intensity is given in units of 10^{-4} MIPs per cm^2 per lost proton. For an A configuration, the shower intensity is given for point losses (P.l.), for the horizontal (two values) and for the vertical loss. The values for direct detection are given, as well as the 'cross-talk' (signal observed at the detector for a loss from the other beam). Distributed loss (D.l.) results are also presented. The loss may be distributed in the case of a loss in the upstream dipole or in the quadrupole. The computations have been done for a distributed loss over 4 m.

Table1. Suitable positions for loss detectors and signal observed for every kind of proton losses for an A configuration. P.l. means point loss and D.l means distributed loss. For focusing quadrupoles (QF) two signals are listed for innermost and outermost losses.

Right Detector	*z (cm)*	-250		200		450
	Intensity(*)	P.l. 640/360	D.l. 520/460	P.l. 100/80	D.l. 100/60	P.l. 100/140 MDCO off 140/140
	Cross-talk(*)	40	40	---	20	---
Left Detector	*z (cm)*	-450		-100		200
	Intensity(*)	P.l. 80		P.l. 120	D.l 80	P.l. 80	D.l. 200
	Cross-talk(*)	---		---	20	---	---

(*) 10^{-4} MIPs/cm^2 per lost proton on the beam screen

Cross-talk signal results to be negligible for all the detectors, consequently the beam which causes the shower is correctly identified.

The values given in Table 1 are used to choose threshold for the BLMs. As a general rule, for safety reasons, the lowest of the possible values are taken. In some cases the most likely value is taken. The final values for the four configurations are put together in Table 2 together with counting values obtained at injection energy. The so obtained normalised counts vary from 80 to 400 $\cdot 10^{-4}$ MIPs/cm^2 per lost proton and the energy ratio varies from 10 to 25.

The proposed location for the BLMs is the same for all configurations. The normalised counting values change however from one configuration to another.

This proposal for the BLMs for the arcs is definitive as long as the LHC arcs layout version is not changed.

Table2. Positions and normalised counting values for the different loss detectors configurations.

TABLE 2A. Positions and normalised counting values for the BLM set. A configuration.

A - DETECTORS	RD1	RD2	RD3	LD1	LD2	LD3
z (cm)	-250	200	450	-450	-100	200
7 TeV counts[2]	400	80	140	80	100	140

TABLE 2B. Positions and normalised counting values for the BLM set. B configuration.

B - DETECTORS	RD1	RD2	RD3	LD1	LD2	LD3
z (cm)	-250	200	450	-450	-100	200
7 TeV counts[2]	400	80	100	100	100	100

TABLE 2C. Positions and normalised counting values for the BLM set. C configuration.

C - DETECTORS	RD1	RD2	RD3	LD1	LD2	LD3
z (cm)	-450	-100	200	-250	200	450
7 TeV counts [2]	100	100	140	360	100	140
450 GeV counts [2]	5	6.5	14	30	6	6

TABLE 2D. Positions and normalised counting values for the BLM set. D configuration.

D - DETECTORS	RD1	RD2	RD3	LD1	LD2	LD3
z (cm)	-450	-100	200	-250	200	450
7 TeV counts [2]	100	100	100	360	100	140

4.2. Quench Protection

Results summarised in Table 2 are of a very general use. The quench alarm thresholds must be calculated for the estimated quench levels at injection and top energy. The final values will be determined by the active surface and detector efficiency of the device used as BLM. We consider the case of 40 MHz PIN diodes with an active surface of 3 mm^2 and an efficiency of 0.6 counts/MIP. Every monitor consists itself of two reverse biased PIN-photodiodes, glued together and red out in coincidence to suppress the noise.

The number of protons which induce a quench caused by local losses is studied in references [8,10]. For medium range transient losses with a time duration of about 10 ms, quench level is $3 \cdot 10^9$ p$^+$s^{-1} at top energy and $3 \cdot 10^{11}$ p$^+$s^{-1} at injection energy for local losses. The uncertainty of these values is about ± 50%.

In Table 2, the normalised counts for the BLMs range from 80 – 400$\cdot 10^{-4}$ MIPs/p$^+$cm^2 at top energy and from 5 – 30$\cdot 10^{-4}$ MIPs/p$^+$cm^2. These values give for the PIN diodes above described counting rates ranging from 144 – 720$\cdot 10^{-6}$ counts/p$^+$ at 7 TeV and from 90 –

[2] 10^{-4} MIPs/cm^2 per lost proton on the beam screen

$540 \cdot 10^{-7}$ counts/p^+ at 450 GeV. The scaling corrector factor between values given in Table 2, MIPs/ p^+cm^2, and counts/ p^+, is $1.8 \cdot 10^{-2}$ counts/(MIPs/cm^2).

The counts in the detectors are compared with their quench alarm threshold (function of the energy of the proton beam). The adequate quench alarm threshold for the prevention of quenching is about a factor 10 less than the quench threshold level. The values in Table 2 must be multiplied by a factor $6.1 \cdot 10^6$ at 7 TeV and by a factor $4.9 \cdot 10^8$ at 450 GeV to obtain quench alarm threshold values in absolute counts/s on the BLMs.

Quench alarm threshold values range from 10^4 to 10^5 counts/s for 7 TeV protons and from 10^5 to 10^6 counts/s for 450 GeV protons.

5. Summary

The proposal for a Beam loss detection system for the LHC arcs has been revised and modified. New geometry according to LHC optics version 6.2 has been defined. New types of geometric configurations were considered. Shower simulations were done with program Geant 3.21 and beam losses conditions and assumptions were made as in previous calculations.

New results show differences in the MIP distribution intensity. In general lower values are obtained for the new version and stronger differences between the showers developed in the SSS-MD and MD-SSS interconnections. The cross-talk signal is slightly different.

An up-to-dated beam loss detection system has been proposed with a set of six Beam Loss Monitors around each Main Quadrupole. The BLMs are placed outside the cryostat in the medium plane. Three BLMs at each side will measure the beam losses of the respective beam. For each LHC arc half-cell, the location of the BLMs is given. Quench threshold levels and quench alarm threshold values have been obtained at top and injection energy.

6. References

1. Arauzo A. and Bovet C., LHC Project Note 213, CERN (2000).
2. Arauzo A. and Bovet C., Proceedings BIW'00, Boston 11th – 15th May 2000.
3. Application Software Group. CERN – CN Division,
   GEANT – Detector Description and Simulation Tool.
4. Minutes 61st Parameters & Layout Committee. http://wwwlhc01.cern.ch/plc/plc.htm
5. Engineering Specification SSS types in the arcs from Q12 to Q12. LHC-LQA-ES-0004.00.
6. Conceptual Layout LHC arcs, optics version 6.1: LHCLSCA-0006. SSS Reference Layout: LHCLQAO-0007.
7. Technical Specification for the supply of superconducting corrector magnets for the LHC: LHC-MO-CI-0001, LHC-MSCB-CI-0001, LHC-MC-CI-0001, LHC-MCDO-CI-0001.
8. J.B. Jeanneret et al., Quench Levels and transient Beam Losses in LHC Magnets, LHC Project Report 44, CERN, 1996.
9. C. Bovet and J.B. Jeanneret, Tertiary beam losses in LHC arcs, LHC Project Note 125, CERN 1997.
10. J.B. Jeanneret, Handling the proton beams above the quench threshold. Proceedings Chamonix X, January 2000.
11. C. Bovet, LHC Project Note 220, CERN (2000).
12. Russenchuck S., *ROXIE Routine for the Optimization of Magnet X-Sections, Inverse Field Calculation and Coil End Design Proceedings*, CERN-99-001, 1998.